INTERMEDIATE STRUCTURE IN THE PHOTONEUTRON AND PHOTOFISSION CROSS SECTIONS IN ^{238}U AND ^{232}Th

O. Y. MAFRA, S. KUNIYOSHI and J. GOLDEMBERG

PUBLICAÇÃO IEA N.º 324
Janeiro — 1974

INSTITUTO DE ENERGIA ATÔMICA
Caixa Postal 11049 (Pinheiros)
CIDADE UNIVERSITÁRIA "ARMANDO DE SALLES OLIVEIRA"
SÃO PAULO — BRASIL

INTERMEDIATE STRUCTURE IN THE PHOTONEUTRON AND PHOTOFISSION CROSS SECTIONS IN ^{238}U AND ^{232}Th*

O. Y. Mafra, S. Kuniyoshi and J. Goldemberg

Coordenadoria de Física Nuclear
Instituto de Energia Atômica
São Paulo - Brasil

Publicação IEA Nº 324
Janeiro - 1974

*Published in Nuclear Physics, A18 6 (1972) L10 - 126

INTERMEDIATE STRUCTURE IN THE PHOTONEUTRON AND PHOTOFISSION CROSS SECTIONS IN ^{238}U AND ^{232}Th

O. Y. Mafra, S. Kuniyoshi and J. Goldemberg

ABSTRACT

The (γ,f) and (γ,n) cross sections in ^{238}U and ^{232}Th and the ratio Γ_n/Γ_f were measured with monochromatic γ-rays, of energies from 5.43 to 9.0 MeV. The competition between the two processes and the implications of the cross-section behaviour are discussed.

1. INTRODUCTION

The intermediate structure observed in the (γ, f) cross sections near the fission threshold has been studied intensively in the last few years. Knowles[1] used Compton-scattered γ-rays from the reaction $^{58}Ni(n,\gamma)^{59}Ni$ as a continuously variable source of γ-rays which presents an overall resolution of $\approx 3\%$ in the range from 5 to 8.3 MeV. Rabotnov et al.[2] used the continuous bremsstrahlung spectrum of a betatron, although difficult to assess the resolution obtained by photo-difference methods in this case, it is probably not better than 10%.

On the other hand, older measurements exist[3,4] using the very high-resolution lines from neutron capture in a variety of elements; the γ-lines in this case are a few eV wide, which can be classified as high resolution. The method of Knowles can be more adequately classified as having intermediate resolution and the bremsstrahlung measurements as having gross resolution.

The existence of intermediate structure near the threshold for the (γ, f) reaction in ^{238}U and ^{232}Th has been clearly established by Rabotnov et al. and by Knowles. Levels of ≈ 200 keV in width have been found in these reactions while in (n, n) reactions only gross structure (≈ 2 MeV in width) is observed. This indicates that the density of states available for energy dissipation in fission near the fission threshold is considerably smaller than the total density of states. As pointed out by Knowles this is understood most conveniently by associating the vibrational states with the second well of an octupole deformation (fig. 1).

The work of Knowles and Rabotnov refers essentially to a few levels in ^{238}U and ^{232}Th, although many levels are expected in any of the possible models.

The method of using monochromatic lines from (n, γ) reactions is a limited one due to the sparseness of available lines but it has the advantage of having a high resolution; the resolution is however not high enough to excite individual levels. In ^{238}U and ^{232}Th one expects at 6 MeV of excitation ≈ 10 levels/eV [ref. [5]] and the (n, γ) lines have a resolution of about 10 eV caused by the Doppler shift. It is expected that the observed cross section will be averaged over the strongly fluctuating microstructure, which will facilitate their interpretation.

A comparison between the data of Manfredini[3,4], Rabotnov[2] and Knowles[1] shows however the existence of discrepancies specially between Manfredini and the other authors.

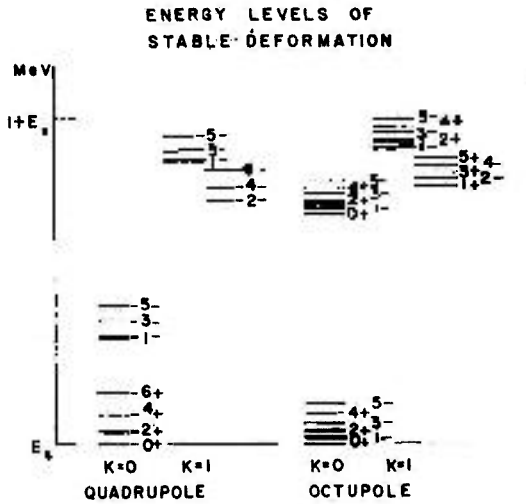

Fig. 1 - Energy levels of stable deformation

For this reason it was decided to repeat the (γ, f) measurements. In addition it was decided to measure the (γ, n) cross sections of the same isotopes in the same experiment in order to study the competition between neutron emission and fission near threshold.

It is known[6] that the ratio Γ_n/Γ_f depends not only on the excitation energy but also on the angular momentum. As the effects of these two factors are different it has not been possible to conclude much about the dependence of Γ_n/Γ_f on the excitation energy from the results of several experiments. Possibly, the better experiments which can be performed to get Γ_n/Γ_f are those in which the compound nucleus is formed by γ-radiation or low-energy neutrons where the angular momentum involved is sufficiently low, so that the excitation-energy dependence is not obscured.

A few measurements of Γ_n/Γ_f have been performed near threshold using the bremstrahlung radiation[7,8] but these experiments have a large error so one cannot conclude much about the variation of the ratio Γ_n/Γ_f with excitation energy.

In 1965 Lindner[9] for the first time used monochromatic γ-radiation to study photoneutron and photofission competition near threshold using radiochemical techniques. Although a correction for the influence of secondary lines was not made, Lindner obtained no definite change of Γ_n/Γ_f in ^{238}U in the energy region from 6 to 9 MeV.

This paper reports our measurements of the Γ_n/Γ_f ratio in ^{238}U and ^{232}Th using monochromatic γ-rays in the energies near threshold, with an experimental arrangement[10,11] completely different from that used by Lindner.

From our data we conclude that, even though at energies above $\approx$ 8.5 MeV the

ratio Γ_n/Γ_f becomes constant, some variation can be seen at low energies.

2. Experimental arrangement

The ratio of the (γ,n) to the (γ,f) cross sections has been determined with neutron capture γ-radiation in several elements used as targets placed near the IEAR-1, 2 MW reactor as can be seen in fig. 2. This experimental arrangement which is employed to produce a high-energy γ-beam with a very low neutron background has been described in detail in refs.[10,11].

The photofission cross section $\sigma_{\gamma,f}$ has been measured with a multiparallel fission chamber containing uranium and thorium electrolytically deposited in oxide form[12]. The neutrons from the (γ, n) and (γ, f) reactions were detected by a 4π long counter of the Halpern type[13], with six BF_3 detectors immersed in paraffin where the neutrons are slowed down. The γ-flux incident on the samples and on the fission chambers was measured with a NaI(Tl) crystal. Fig. 3 shows the schematic arrangement of the detectors.

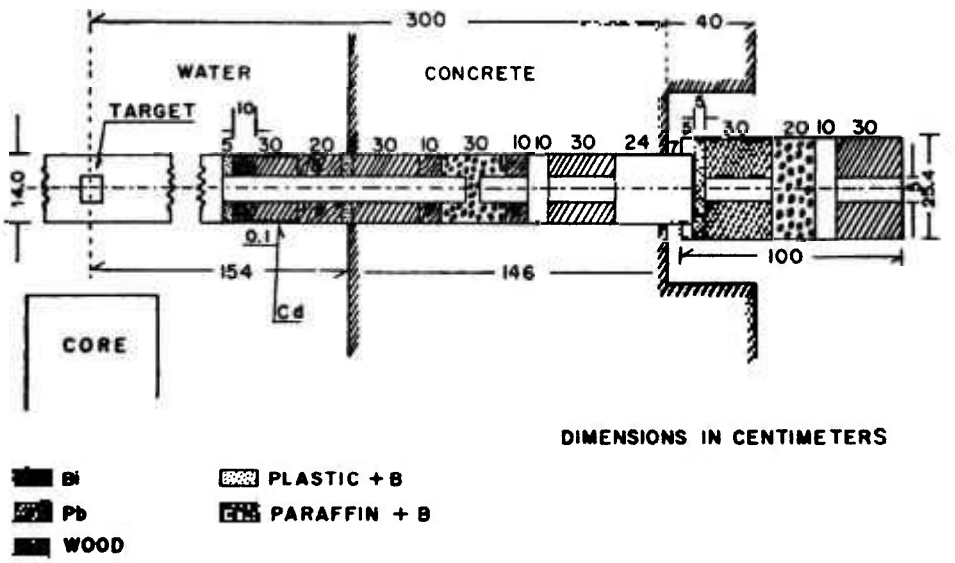

Fig. 2 - Experimental arrangement for γ-radiation production.

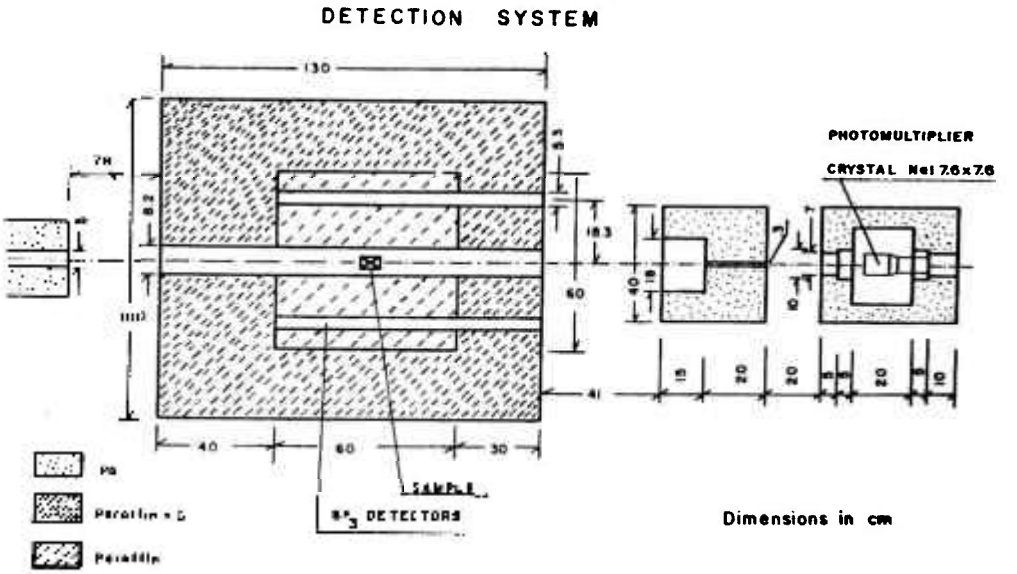

Fig. 3 - Detection system.

The fission-chamber efficiency was determined by a comparison of one measurement at an energy where only fission occurs with the counting rate of the long-counter detector; this counter was calibrated using a standard source of $^{24}Na + {}^{2}H_2O$.

The neutrons scattered in the target used to produce the γ-lines have been subtracted using a graphite target where the γ-lines do not have sufficient energy to produce reactions in ^{238}U and ^{232}Th. The scattering was then calculated for all the other targets using the respective masses and neutron scattering cross sections.

TABLE 1

Targets employed, principal γ-ray energies, flux incident on the samples

Element	Energy (MeV)	$\phi(\gamma/cm^2\ sec)$
^{32}S	5.43	$(2.6 \pm 0.2) \times 10^4$
^{89}Y	6.07	$(7.3 \pm 0.7) \times 10^3$
^{40}Ca	6.42	$(6.8 \pm 0.7) \times 10^3$
^{48}Ti	6.73	$(7.7 \pm 0.6) \times 10^4$
^{9}Be	6.83	$(8.5 \pm 1.1) \times 10^2$
^{55}Mn	7.23	$(3.5 \pm 0.4) \times 10^4$
^{207}Pb	7.38	$(2.8 \pm 0.3) \times 10^3$
^{56}Fe	7.64	$(2.8 \pm 0.3) \times 10^4$
^{27}Al	7.72	$(1.4 \pm 0.1) \times 10^4$
^{64}Zn	7.88	$(1.1 \pm 0.1) \times 10^4$
^{63}Cu	7.91	$(2.8 \pm 0.3) \times 10^4$
^{85}Ni	9.00	$(1.5 \pm 0.1) \times 10^4$

The targets employed, the main line energy and the γ-flux incident on the uranium and thorium samples are listed in table 1. We have used natural uranium, so the cross sections measured are not only those corresponding to ^{238}U. However since the photofission cross sections in ^{235}U and ^{238}U are of the same order of magnitude the error committed on this assumption is of the order of the quantity of ^{235}U in the natural uranium or ≈ 0.7%.

3. Results

The photofission cross sections are related to the experimental counting rates by a system of linear equation:

$$\sum r_i \sigma_i = N_f / \phi_p N_t , \qquad (1)$$

where σ_i is the photofission cross section at the energy of the ith line of the γ-ray spectrum emited by the reactor target, r_i is the γ-ray flux of the ith line relative to the main line, N_f is the number of fissions per sec corrected for background, ϕ_p is the main line flux in photons · cm^{-2} · sec^{-1} and N_t is the number of uranium or thorium atoms.

This set of linear equations can be solved only with some approximations. Once the solution of the quadratic system obtained from the principal lines of the elements is calculated, a linear interpolation is made between the first set of solutions, and this procedure may be repeated until the variations introduced are very small.

In order to test this method of analysis the deuterium (γ,n) cross section was measured using the same experimental arrangement. The results obtained are in reasonable agreement

with the theoretical cross section for deuterium as can be seen in fig. 4.

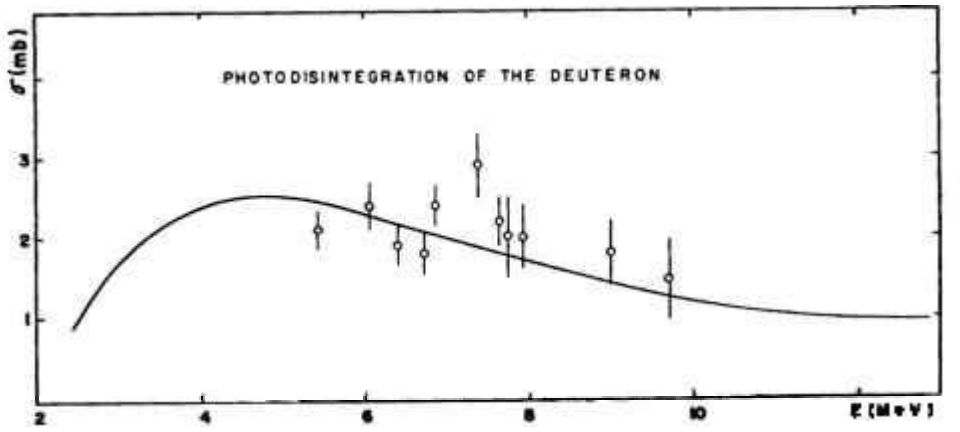

Fig. 4 - Deuterium cross sections obtained from neutron capture sources compared with the theoretical values.

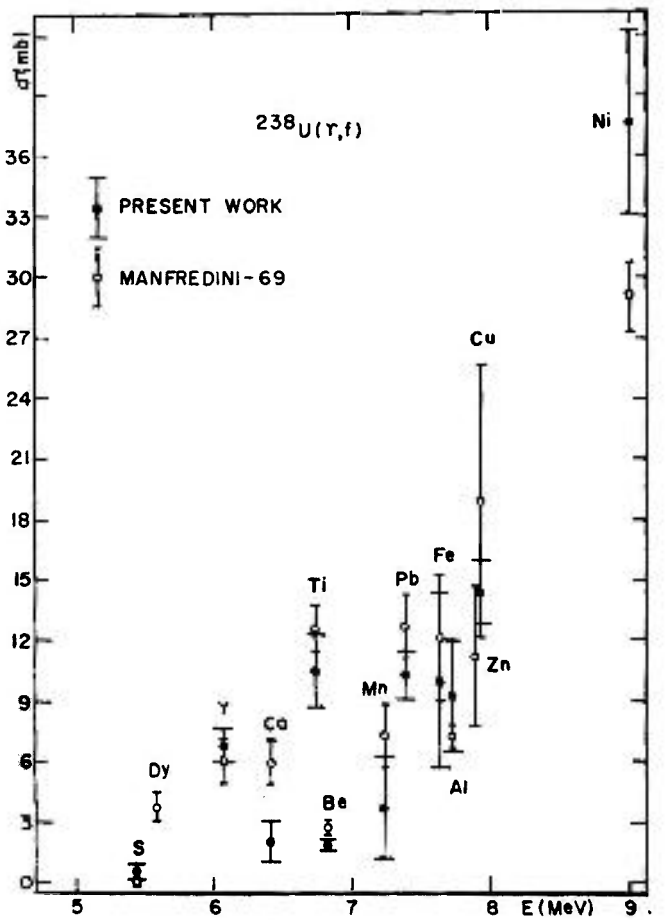

Fig. 5 - Photofission cross sections of ^{238}U compared with Manfredini's results. Element symbols indicate the sources of neutron capture γ-rays whose energies are listed in table I.

The cross sections obtained[14] for the (γ, f) reaction in ^{238}U and ^{232}Th are given in figs. 5-7 and table 2 and the structure obtained confirms previous measurements made with γ-lines[1,4].

The results obtained for titanium (6.73 MeV) and beryllium (6.83 MeV) targets have been checked a number of times because of the large differences found in these cross sections. The beryllium target gave a very high background due to a large neutron scattering cross section and low threshold for (γ, n) reactions. However the (γ,f) cross section obtained for the beryllium line is very low even without any correction for the background which would overestimate its real value.

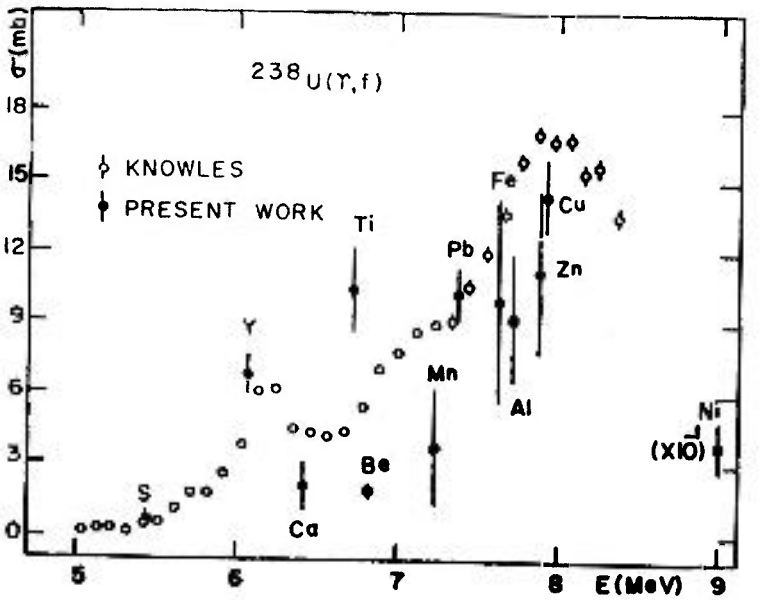

Fig. 6 - Photofission cross sections of ^{238}U compared with Knowles's results. Element symbols indicate the sources of neutron capture γ-rays whose energies are listed in table 1.

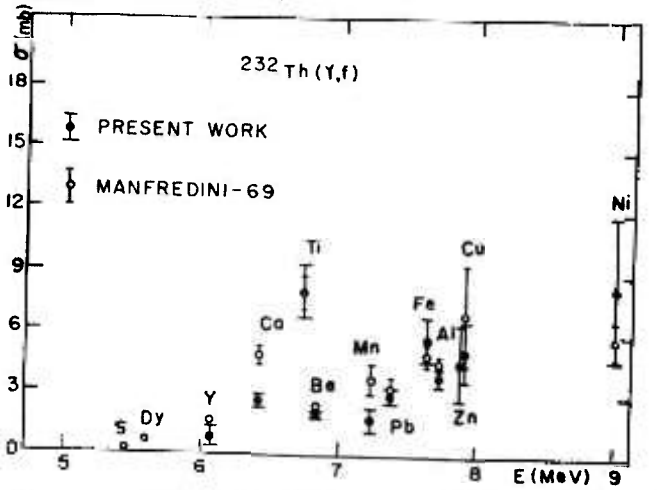

Fig. 7 - Photofission cross sections of ^{232}Th compared with Manfredini's results. Element symbols indicate the sources of neutron capture γ-rays whose energies are listed in table 1.

The total cross section for neutron emission is given by

$$\sigma_{\gamma,N} = \sigma_{\gamma,n} + 2\sigma_{\gamma,2n} + 3\sigma_{\gamma,3n} + \quad + \nu\sigma_{\gamma,f} + (1+\nu)\sigma_{\gamma,nf} + (2+\nu)\sigma_{\gamma,2nf} + \quad .$$

where ν is the number of neutrons emitted per fission obtained for one target. Utilizing the long counter what is measured is only

$$\sigma_{\gamma,N} = \sigma_{\gamma,n} + \nu\sigma_{\gamma,f} \qquad (2)$$

TABLE 2

Targets employed, principal γ-ray energies and uranium and thorium photofission cross sections with experimental errors

b	Elements	E(MeV)	$\sigma_{\gamma,f}$(mb) uranium	$\sigma_{\gamma,f}$(mb) thorium
	^{32}S	5.43	0.53 ± 0.42	0.10 ± 0.08
	^{89}Y	6.07	6.78 ± 0.75	0.82 ± 0.57
	^{40}Ca	6.42	2.1 ± 1.0	2.6 ± 0.3
	^{48}Ti	7.63	10.4 ± 1.7	8.00 ± 1.3
	^{9}Be	6.83	1.9 ± 0.2	2.0 ± 0.2
	^{55}Mn	7.23	3.7 ± 2.4	1.8 ± 0.6
	^{207}Pb	7.38	10.2 ± 1.1	2.9 ± 0.4
	^{56}Fe	7.64	10.0 ± 4.3	5.7 ± 1.1
	^{27}Al	7.73	9.2 ± 2.6	3.8 ± 0.4
	^{64}Zn	7.88	11.1 ± 3.4	4.6 ± 1.8
	^{63}Cu	7.91	14.3 ± 1.5	5.1 ± 1.4
	^{58}Ni	9.00	37 ± 11	8.4 ± 3.5

because the γ-energies at which we are working are below the threshold for the other reactions. Substituting eq. (2) in eq. (1) one obtains.

$$\frac{CA}{\epsilon m N_0 \phi_p} = (\sigma_{\gamma,n} + \nu\sigma_{\gamma,f})_1 + (\sigma_{\gamma,n} + \nu\sigma_{\gamma,f})_2 r_2 + \quad + (\sigma_{\gamma,n} + \nu\sigma_{\gamma,f})_p \qquad (3)$$

where C is the counts/unit time, A the mass number, N_0 Avogadro's number, m the sample mass, ϵ the long-counter efficiency, ϕ_p the main line flux and r_i the γ-ray flux of the ith line relative to the main line.

The solution of this linear system gives the total neutron production cross section

$$\sigma_{\gamma,N} = \sigma_{\gamma,n} + \nu\sigma_{\gamma,f}$$

which can be seen in figs. 8 and 9.

The total cross section for neutron emission is given by

$$\sigma_{\gamma,N} = \sigma_{\gamma,n} + 2\sigma_{\gamma,2n} + 3\sigma_{\gamma,3n} + \quad + \nu\sigma_{\gamma,f} + (1+\nu)\sigma_{\gamma,nf} + (2+\nu)\sigma_{\gamma,2nf} + \quad .$$

where ν is the number of neutrons emitted per fission obtained for one target. Utilizing the long counter what is measured is only

$$\sigma_{\gamma,N} = \sigma_{\gamma,n} + \nu\sigma_{\gamma,f} \tag{2}$$

TABLE 2

Targets employed, principal γ-ray energies and uranium and thorium photofission cross sections with experimental errors

b	Elements	E(MeV)	$\sigma_{\gamma,f}$(mb) uranium	$\sigma_{\gamma,f}$(mb) thorium
	^{32}S	5.43	0.53 ± 0.42	0.10 ± 0.08
	^{89}Y	6.07	6.78 ± 0.75	0.82 ± 0.57
	^{40}Ca	6.42	2.1 ± 1.0	2.6 ± 0.3
	^{48}Ti	7.63	10.4 ± 1.7	8.00 ± 1.3
	^{9}Be	6.83	1.9 ± 0.2	2.0 ± 0.2
	^{55}Mn	7.23	3.7 ± 2.4	1.8 ± 0.6
	^{207}Pb	7.38	10.2 ± 1.1	2.9 ± 0.4
	^{56}Fe	7.64	10.0 ± 4.3	5.7 ± 1.1
	^{27}Al	7.73	9.2 ± 2.6	3.8 ± 0.4
	^{64}Zn	7.88	11.1 ± 3.4	4.6 ± 1.8
	^{63}Cu	7.91	14.3 ± 1.5	5.1 ± 1.4
	^{58}Ni	9.00	37 ± 11	8.4 ± 3.5

because the γ-energies at which we are working are below the threshold for the other reactions. Substituting eq. (2) in eq. (1) one obtains.

$$\frac{CA}{\epsilon m N_0 \phi_p} = (\sigma_{\gamma,n} + \nu\sigma_{\gamma,f})_1 r_1 + (\sigma_{\gamma,n} + \nu\sigma_{\gamma,f})_2 r_2 + \quad + (\sigma_{\gamma,n} + \nu\sigma_{\gamma,f})_p \tag{3}$$

where C is the counts/unit time, A the mass number, N_0 Avogadro's number, m the sample mass, ϵ the long-counter efficiency, ϕ_p the main line flux and r_i the γ-ray flux of the ith line relative to the main line.

The solution of this linear system gives the total neutron production cross section

$$\sigma_{\gamma,N} = \sigma_{\gamma,n} + \nu\sigma_{\gamma,f}$$

which can be seen in figs. 8 and 9.

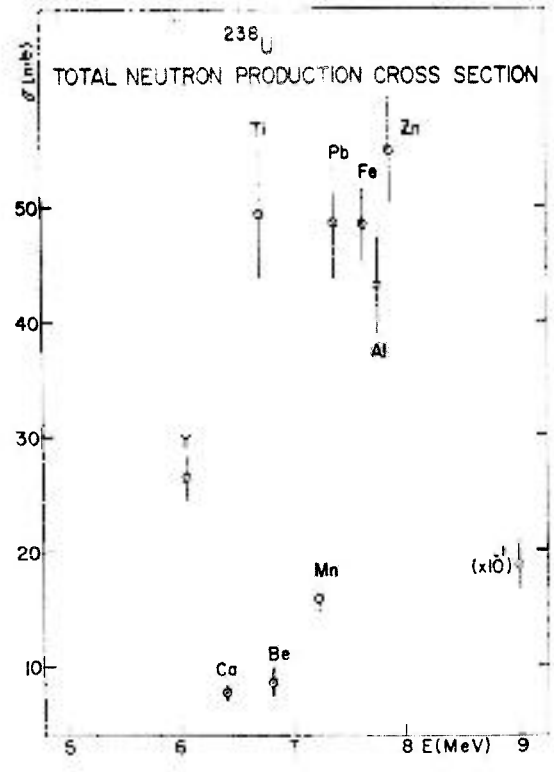

Fig. 8 - Total neutron production cross section for ^{238}U. Element symbols indicate the sources of neutron capture γ-rays whose energies are listed in table 1.

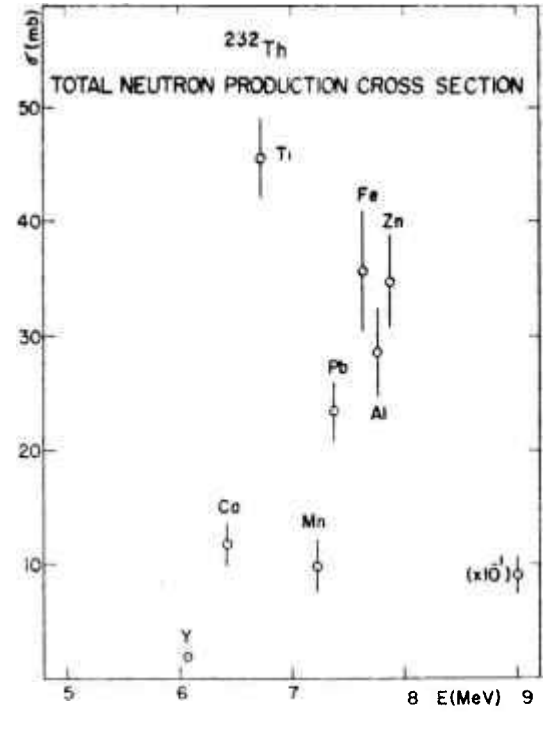

Fig. 9 - Total neutron production cross section for ^{232}Th. Element symbols indicate the sources of neutron capture γ-rays whose energies are listed in table 1.

TABLE 3

Principal γ-ray energies and uranium and thorium (γ,n) cross sections

E(MeV)	$\sigma_{\gamma,n}$(mb) uranium	$\sigma_{\gamma,n}$(mb) thorium
6.07	9.0 ± 2.7	
6.42	2.2 ± 1.1	5.1 ± 2.0
6.73	22.7 ± 6.3	25.7 ± 4.1
6.83	3.7 ± 1.2	
7.23	6.3 ± 3.9	5.3 ± 2.5
7.38	22.2 ± 5.5	16.1 ± 2.6
7.64	22.6 ± 7.2	21.6 ± 5.3
7.72	19.6 ± 4.3	19.2 ± 3.9
7.88	26.5 ± 6.7	23.4 ± 4.2
9.00	93.6 ± 25.5	69.6 ± 16.4

TABLE 4

Principal γ-ray energies and uranium and thorium Γ_n/Γ_f ratios

E(MeV)	Uranium Γ_n/Γ_f	Thorium Γ_n/Γ_f
6.07	1.3 ± 0.4	
6.42	1.1± 0.5	2.0 ± 0.8
6.73	2.1 ± 0.6	3.2 ± 0.6
6.83	1.9 ± 0.6	
7.23	1.7 ± 1.1	2.9 ± 1.4
7.38	2.1 ± 0.5	5.5 ± 1.0
7.64	2.2 ± 0.8	3.8 ± 0.9
7.72	2.1 ± 0.4	5.1 ± 1.0
7.88	2.3 ± 0.7	5.1 ± 1.0
9.00	2.5 ± 0.7	8.3 ± 2.0

Assuming that $\nu = 2.5$ neutrons because this value for the energies employed here (up to 9 MeV) does not have strong variations[15], and using the $\sigma_{\gamma,f}$ previously determined we obtain the $\sigma_{\gamma,n}$ cross sections in ^{238}U and ^{232}Th as can be seen in figs. 10 and 11 and in table 3†.

In these results we see the existence of a structure also in the (γ, n) cross sections which has not been seen before because the existing measurements of $\sigma_{\gamma,n}$ were made with low-resolution bremsstrahlung.

Once we know $\sigma_{\gamma,n}$ and $\sigma_{\gamma,f}$, we can calculate

$$\Gamma_n/\Gamma_f = \sigma_{\gamma,n}/\sigma_{\gamma,f}.$$

The data obtained can be seen in figs. 12 and 13, and table 4 for ^{238}U and ^{232}Th. For purposes of comparison, fig. 12 also shows Lindner's[9] results for ^{238}U.

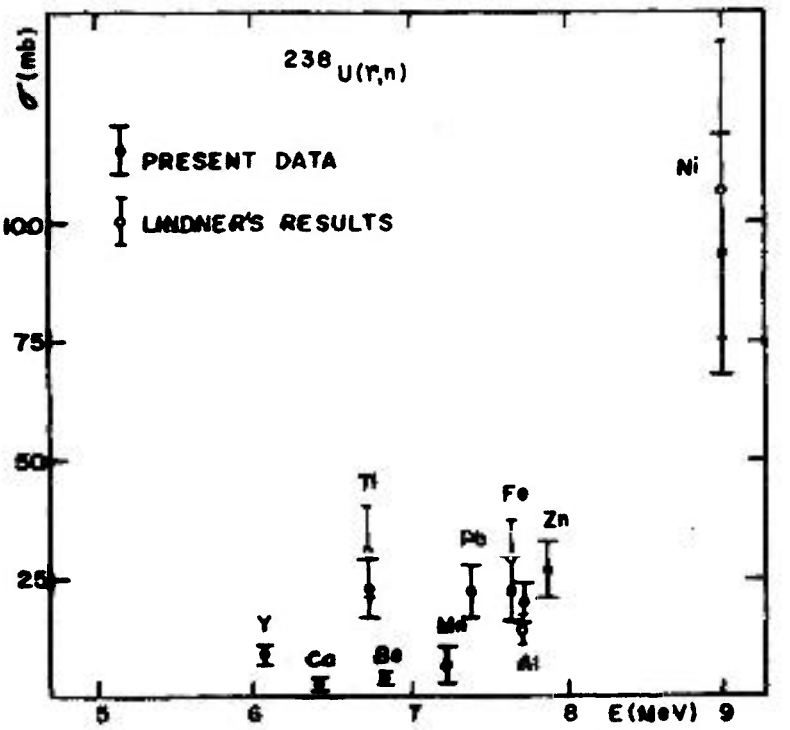

Fig. 10 - Photoneutron cross sections of ^{238}U compared with Lindner's results. Element symbols indicate the sources of neutron capture γ-rays whose energies are listed in Table 1.

† The neutron separation energy of ^{238}U from atomic mass tables is 6.058 ± 0.040 MeV [1965 assessment[22]] and 6.147 ± 0.040 according to the most recent (1966) assessment[23]. The present measurement of the $\sigma(\gamma,n)$ cross section of ^{238}U at 6.07 MeV puts an upper limit on the neutron separation energy in disagreement with the (1966) assessment. (This was pointed out to us by J.W. Knowles.)

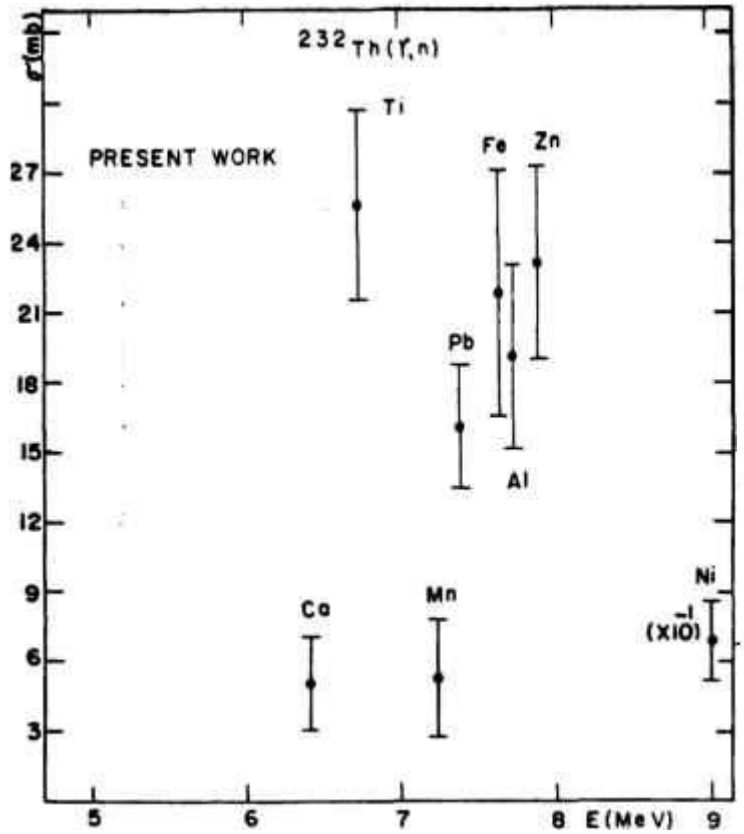

Fig. 11 - Photoneutron cross sections of ^{232}Th. Element symbols indicate the sources of neutron capture γ-rays whose energies are listed in table 1.

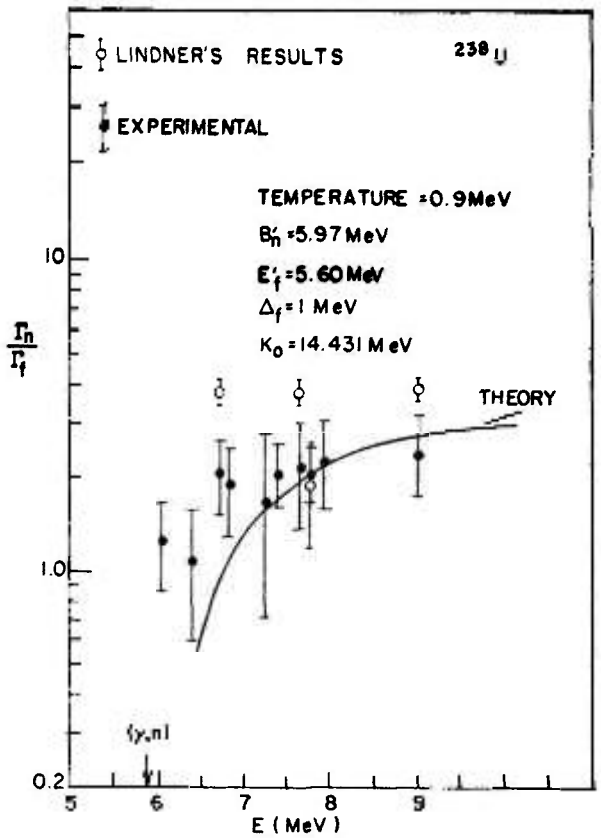

Fig. 12 - Experimental values of Γ_n/Γ_f compared with the theoretical predictions.

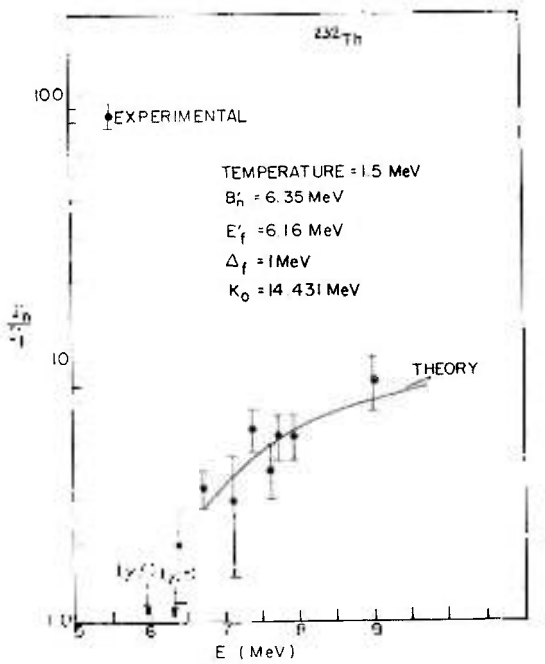

Fig. 13 - Experimental values of Γ_n/Γ_f compared with the theoretical predictions.

4. Discussion

Although our data is affected by apreciable errors some features stand out clearly:

(i) The same structure present in the (γ, f) cross sections (figs. 5 and 7) is seen in the (γ,n) cross sections (figs. 10 and 11). No (γ, n) results excepts the old bremsstrahlung[16] results are available in the literature. This intermediate structure is somewhat surprising because in the (γ,f) cross sections it has been attributed to the small number of states leading to fission; to find the same structure in the (γ, n) cross sections indicates that the same states are involved in this process, which is somewhat unexpected. Tentatively one would be tempted to say that the neutrons are emitted mainly from the deformed nucleus on its way to scission and not from the excited undeformed nucleus. One should notice in connection with this point that in the photofission of ^{238}U and ^{232}Th the ratio Γ_n/Γ_f is of the order of 1 when it becomes constant (9 MeV), as discussed below, indicating that the mean lives for the (γ, n) and (γ, f) processes are of the same order of magnitude.

(ii) In addition to the peak at $\approx$ 6.2 MeV which is well established and studied by Knowles, our data indicates another peak at 6.73 MeV corresponding to the γ-ray emitted in the neutron capture of ^{48}Ti. Experimentally there seems to be no doubt that the cross section at this energy is larger than the cross sections at the adjoining energies 6.83(^{9}Be) and 6.42 (^{40}Ca) MeV. This peak is not seen by Knowles. It is conceivable that due to the high-resolution nature of these measurements, this point is unusually high due to a coincidence in the energies of the γ-ray used and that of a sharp level. This structure would not be observed in intermediate or gross structure measurements. In fig. 14 resolution functions of 1% and 5% were folded into

the present data to see the effect of the poorer resolution on the cross section; clearly the shape obtained tends to become more similar to the one obtained by Knowles.

(iii) In figs. 12 and 13 we compared the results obtained for the ratio $\sigma_{(\gamma, n)}/\sigma_{(\gamma, f)}$ to the theoretical expectation for Γ_n/Γ_f.

The fission width Γ_f was calculated theoretically using the expression[17,18]

$$\Gamma_f = \frac{1}{2\pi} \frac{N^*}{\rho} \quad (4)$$

where N^* is the effective number of channels at the barrier and ρ is the density of levels. In this formula N^* is given by

$$N^* = \int_0^{E - E'_f} \rho^*(E - E'_f - \epsilon)\, d\epsilon. \quad (5)$$

where ρ (E) is the compound nucleus density of levels before fission, $\rho^*(E-E'_f-\epsilon)$ is the density of levels at the saddle point, E'_f is the effective fission threshold taking into account the even- or odd-nuclei character and E is the excitation energy. The effect of the double-humped barrier for fission does not seem to be important in the calculation of Γ_f. If we consider the two barriers we must specify the effective number of channels in the two wells (fig. 15) and we get[19,20]

$$\langle \Gamma_f \rangle = \frac{1}{2\pi\rho} \frac{N_A \times N_B}{N_A + N_B} \quad (6)$$

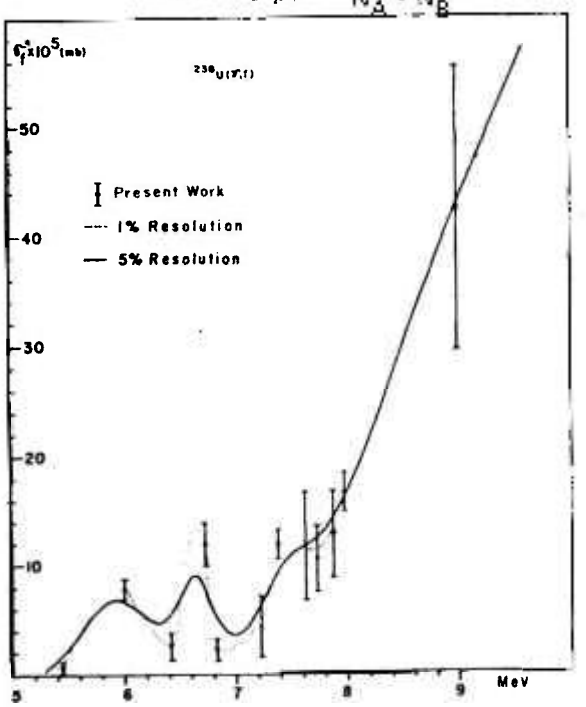

Fig. 14 - Photofission cross sections folded with 1% and 5% resolution functions

where N_A and N_B are the effective number of channels at the barriers A and B. From experimental data we can see[19,21] that $N_A \approx 0.5$ and $N_B \approx 0.002$ so $N_A \gg N_B$ and

$$\Gamma_f = \frac{1}{2\pi\rho_1} \frac{N_B}{1 + N_B/N_A}, \tag{8}$$

which is the same expression we have used without considering this correction.

The neutron whidt was also calculated theoretically using Weisskopf's evaporation theory According to this theory we can calculate the probability per unit time $\omega_n(\epsilon)\, d\epsilon$ of a nucleus A, excited to an energy E_A, emitting a neutron with a knetic energy between ϵ and $\epsilon + d\epsilon$ and to become a nucleus B with an excitation energy $E_B = E_A - B_n - \epsilon$, where B_n is the neutron binding energy;

$$\Gamma_n = h \int_0^{E - B'_n} \omega_n(\epsilon) d\epsilon,$$

where

$$\omega_n[\epsilon]d\epsilon = \frac{\sigma(E_A, \epsilon)}{\pi^2 h^3} \frac{gm\epsilon\rho(E - B'_n - \epsilon)d\epsilon}{\rho(E)}, \tag{9}$$

and where $\sigma(E_A, \epsilon)$ is the inverse cross section, m the neutron mass, g =2 for neutrons, $\rho(E)$ is the compound nucleus density of levels, and $\rho(E - B'_n - \epsilon)$ the residual nucleus density of levels.

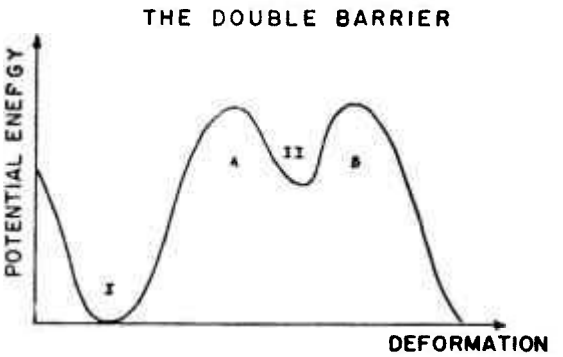

Fig. 15 - The double-humped barrier.

If we make an hypothesis about the density of levels we can calculate the ratio Γ_n/Γ_f We have used

$$\rho = C \exp(E/T), \tag{10}$$

(where T is the nuclear temperature) given by Huizenga[6] because it was found that this was the formula which gave the best agreement with our experimental data. The Fermi-gas formula did

not agree as well with our results.

Performing the necessary integrations in expressions (5) and (8) one gets

$$\Gamma_n/\Gamma_f = \frac{2TA^{2/3}}{K_0} \cdot \frac{-1-(E-B_n)/T + \exp((E-B_n)/T)}{1-\exp((E-E'_f)/T)} \qquad (11)$$

where K_0 = 14.431 MeV.

In figs. 12 and 13 the theoretical results are plotted with our data. Above 9 MeV the ratio Γ_n/Γ_f seems to be constant but below this energy one sees clearly a variation with energy. Data derived from Lindner's data is also plotted in fig. 12.

The present data at 9 MeV where this ratio reaches a constant value is also compared with the data of other authors in figs. 16 and 17.

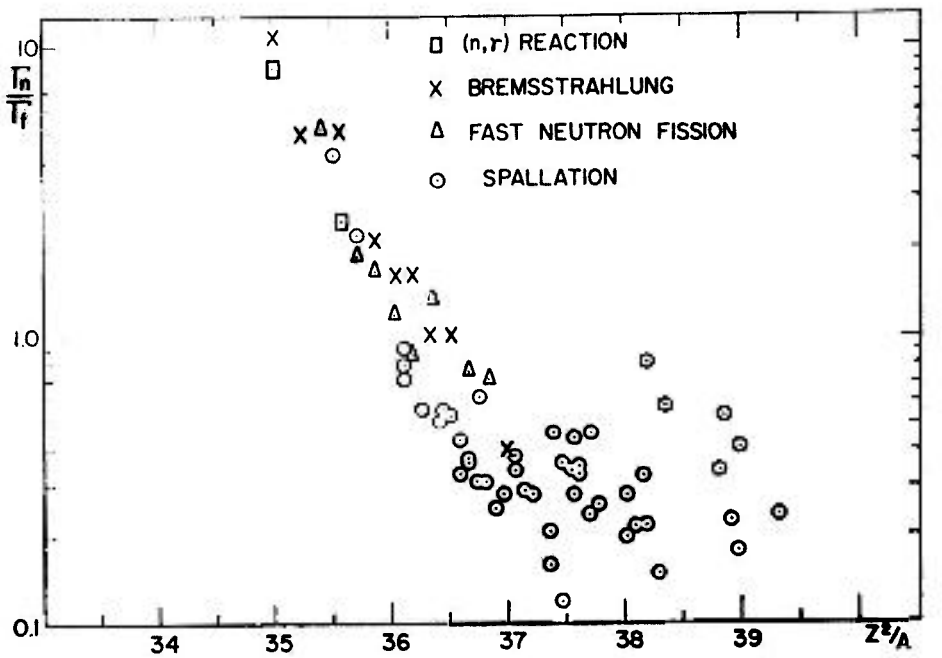

Fig. 16 - Variation of the Γ_n/Γ_f ratio with the fissionability parameter.

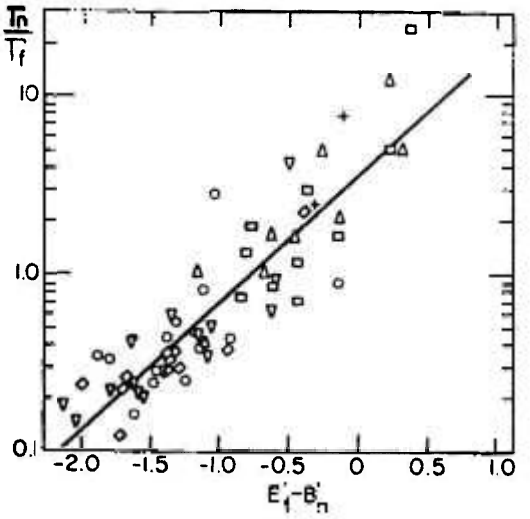

Fig. 17 - Variation of the Γ_n/Γ_f ratio with the difference of the photofission and the photoneutron threshold.

One should notice that the data for uranium and thorium is best fitted for nuclear temperatures of 0.9 MeV and 1.5 MeV, respectively. This difference in temperature is quite surprising and might be due to a deformation of the compound nucleus which would cool it prior to neutron emission.

Measurements of the (γ, n) cross section using a radiochemical separation of ^{237}U from the fission fragments are in progress in order to clarify independently the important structure exhibited in the process.

We acknowledge Prof. Ross A. Douglas' useful comments.

RESUMO

As seções de choque (γ, f) e (γ, n) e a razão Γ_n/Γ_f para o ^{238}U e ^{232}Th foram medidas com raios gama monocromáticos de energias no intervalo de 5,43 a 9,0 MeV.

A competição entre os dois processos envolvidos e as implicações que resultam do comportamento das seções de choque são discutidas.

RÉSUMÉ

On a mesuré les sections efficaces (γ, f) et (γ, n) et la relation Γ_n/Γ_f pour les isotopes ^{238}U et ^{232}Th avec les rayons γ monocromatiques d'energies 5,43 à 9,0 MeV.

On a discuté aussi la competition entre ces deux procèssus et les implications qui resultent des valeurs obtenues pour les sections efficaces.

REFERENCES

1) A. M. Khan and J. M. Knowles, Nucl. Phys. **A179** (1972) 333
2) N. S. Rabotnov et al., Sov. J. Nucl. Phys. **11** (1970) 285
3) A. Manfredini et al., Nuovo Cim. **B44** (1966) 218
4) A. Manfredini et al., Nucl. Phys. **A127** (1969) 687
5) J. M. Blatt and V. F. Weisskopf, Theoretical nuclear physics (Wiley, New York, 1952) ch. VIII nº 6
6) P. Endt, Nuclear reactions vol. 2 (North-Holland, Amsterdam, 1962) p. 42
7) E. K. Hyde, The nuclear properties of heavy elements vol 3 (Englewood Cliffs, Prentice Hall, 1964) chs. 13 and 10
8) R. Vandenbosch and J. R. Huizenga, Proc. of the Second United Nations Conf. on peaceful uses of atomic energy, Geneva, 1958, vol. 15, p. 284
9) M. Lindner, Nucl. Phys. **61** (1965) 17
10) O. Y. Mafra, Master thesis, São Paulo, 1969
11) O. Y. Mafra, Doctor thesis, São Paulo, 1971
12) O. Y. Mafra and F. G. Bianchini, São Paulo, IEA 145, 1967
13) H. M. Gerstenberg and E. C. Fuller, US Departament of Commerce-National Bureau of Standards, NBS-416, 1967
14) O. Y. Mafra and S. Kuniyoshi, Academia Brasileira de Ciências **43**, nº 3 (1971)
15) J. C. Hopkins and B. C. Diven, Nucl. Phys. **48** (1963) 433
16) J. E. Gindler and J. R. Huizenga, Phys. Rev. **104** (1956) 425
17) N. Bohr and J. A. Wheeler, Phys. Rev. **56** (1939) 426
18) Fast neutron physics, ed. J. B. Marion and J. R. Fowler (Wiley, New York - London, 1963) ch. V.S., p. 2051
19) J. Pedersen, The fission process, III Simpósio Brasileiro de Física Teórica, Rio de Janeiro, fasc. IV, 1970
20) S. Bjørnholm and V. M. Strutinsky, Nucl Phys. **81** (1966) 1
21) E. Migneco and J. P. Theobald. Nucl. Phys. **A112** (1968) 603
22) J. H. E. Mattauch, W. Threle and A. H. Wapstra, Nucl. Phys. **67** (1965) 1
23) C. Maples, G. W. Goth and J. Cemy, Nucl. Data **2** (1966) 610